Engineering Structures 278 (2023) 115515

Contents lists available at ScienceDirect

Engineering Structures

journal homepage: www.elsevier.com/locate/engstruct

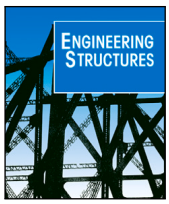

Short communication

Wind-induced fragility of a monopole structure via Artificial Neural Network based surrogate analysis

Lei Zhang[1], Luca Caracoglia [*,1]

Department of Civil and Environmental Engineering, Northeastern University, Boston, MA 02115, USA

ARTICLE INFO

Keywords:
Surrogate modeling
Artificial neural networks
Fragility analysis
Slender monopole structure

ABSTRACT

Although brute-force Monte Carlo (BFMC) sampling has been commonly used in performance-based wind engineering (PBWE) due to its robustness and efficiency, the computing cost required by the considerable amounts of repetitious, stochastic realizations for situations that involve large structures and a multitude of uncertainties is still prohibitive. To alleviate the computational burden, this communication proposes a surrogate modeling approach, based on artificial neural networks (ANNs), to evaluate the probabilistic integral required to quantify wind-induced fragilities. The resultant ANN models form a computationally viable alternative between input and output variables, based on a database of observations obtained through BFMC stochastic simulations. A preliminary study is conducted to examine the fragility of a slender, monopole tower structure under the excitation of multidirectional, mixed-climate wind loads. The ANN-powered surrogate results show adequate accuracy while drastically reducing the computing time to less than 1% of the cost of BFMC approach. It is promising to incorporate the surrogate ANN modeling in a PBWE framework.

1. Introduction

1.1. State of the art

Performance-based wind engineering (PBWE) has emerged as an appealing approach to evaluate environmental risks on civil structures and infrastructures, induced by wind-related hazards [1–9]. Adapted from the methodology of performance-based engineering that was initially developed for seismic structural design by the Pacific Earthquake Engineering Research (PEER) Center [10], the probabilistic approach termed PBWE provides a rational and consistent analysis method for addressing uncertainties [11] arising from the natural hazard, the structure and their complex interactions [12–14]. It consists of deriving a series of logical elements associated with hazard analysis, structural/non-structural analysis, damage analysis and loss analysis [15]. Contrary to conventional prescriptive-based approaches, PBWE focuses on the construction of a structure to meet pre-selected performance objectives or limit states.

Uncertainties examined by PBWE incorporate aleatory uncertainties (e.g., related to the inherently random nature of wind load properties) and epistemic uncertainties (e.g., inappropriate simplification of analysis models, incomplete definition of structural parameters or inadequate modeling of fragilities). Quantification of these uncertainties needs evaluating the PEER probabilistic integral and normally relies on Monte Carlo sampling because of its robustness; more importantly, no constraints are imposed on the complexity of the assumed numerical and probability models [16,17]. However, it is still extremely expensive to generate the required number of repetitions or stochastic realizations, despite the recent growth in computational power. Sampling often involves large nonlinearity and multi-dimensionality in the design variables, hazard intensity measures and their mutual interaction, and hence requires considerable amounts of dedicated computer time.

To address this limitation, surrogate modeling (also known as meta-modeling) has been proposed as a feasible alternative to accelerate the evaluation of the structural dynamic response. It has been successfully incorporated in simulation-based frameworks for structural performance assessment, subject to natural hazards [18–20]. Using a dataset of initial observations, obtained through a high-fidelity simulation model, surrogate models offer a computationally inexpensive approach to reproduce the mapping between input and output variables of the original system [21]. The most commonly used surrogate modeling scheme that reproduces the mapping is regression or interpolation using, e.g., polynomials [22–24], radial basis functions and Kriging [19,25–27], support vector machines [27–29] and artificial neural networks (ANNs) [28,30–34].

* Corresponding author at: Department of Civil and Environmental Engineering, Northeastern University, 400 Snell Engineering Center, 360 Huntington Avenue, Boston, MA 02115, USA.
E-mail address: lucac@coe.neu.edu (L. Caracoglia).
[1] Authors equally contributed to the work described herein.

https://doi.org/10.1016/j.engstruct.2022.115515
Received 9 October 2021; Received in revised form 8 December 2022; Accepted 19 December 2022

Surrogate modeling has gained its popularity in the wind engineering community for the rapid evaluation of wind-excited responses. Le and Caracoglia [35] proposed an ANN-based model to investigate the performance of structures exposed to tornadic wind loads. Micheli et al. [36] examined Kriging surrogate models and adaptive wavelet networks for the design of tall buildings under extreme wind loads. Chuang and Spence [37] proposed a surrogate model that combines nonlinear, auto-regressive with exogenous input (NARX) models and modal-basis reduction to estimate the nonlinear response of a multi-degree-of-freedom structure subject to multivariate stochastic wind loads. Since the duration of wind excitation is relatively long, the sequence-to-sequence mapping between wind loads and wind-induced response can be captured by long–short term memory (LSTM) neural networks. Surrogate modeling through physics-informed LSTM network, where the physical information derives from the equation of motion, exhibits a satisfactory accuracy in simulating the dynamics of wind-excited structures [38,39]. In addition, the LSTM network combined with model order reduction that preserves the coupling effects by further increasing the computational efficiency, has been used to model nonlinear dynamic systems subject to stochastic excitation [40,41]. A convolutional neural network-based surrogate model was also employed to predict response time histories of a transmission tower under complex wind load conditions [42].

1.2. Motivation and objectives

Despite the extraordinary predictive capabilities of ANNs and their numerous applications in civil engineering [43], the surrogate neural network modeling in the context of PBWE is still rare. Thus, this work presents a preliminary study using ANN to conduct surrogate fragility analysis in a PBWE simulation framework, with the goal to alleviate the computational burden accompanying standard brute-force Monte-Carlo based simulations. This study illustrates and examines systematic implementation of ANN surrogate models to facilitate computationally inexpensive evaluation of structural fragility. In particular, the study will examine the performance of a slender, monopole tower (plate) structure subjected to turbulent wind loads. The study utilizes a slender, monopole tower structure with concentrated wind load against multi-directional, mixed-climate winds; the goal is to build more efficient PBWE simulations that can efficiently analyze risks for structural systems susceptible to wind hazards. The dataset of initial observations is obtained from stochastic simulations using a detailed physics-based model, which needs high up-front cost. Nevertheless, once the ANN models are calibrated (i.e., trained, validated, and tested), they enable evaluation of structural performance under a similar type of excitation with minimum effort. Numerical ANN results are verified against fragility results obtained from high-fidelity BFMC simulations, and subsequently compared to the results found by the Layered Stochastic-Approximation Monte-Carlo (LSAMC) algorithm, a method recently proposed by the authors [44] to evaluate the PEER probabilistic integral for risk assessment. In summary, this study entails the execution of the following objectives:

1. Generate a low-fidelity, low-resolution dataset and a high-fidelity, high-resolution dataset, featuring differentiated sample sizes, used for the calibration and the validation of the surrogate neural network models.
2. Verify the surrogate ANN results in the context of wind-induced fragility of a monopole structure through comparison against two Monte-Carlo based methods: BFMC sampling and LSAMC method.
3. Investigate the feasibility of including surrogate ANN models in a PBWE framework with reduced computational cost.

2. Background theory

2.1. Multi-directional aerodynamic load and response analysis

As a linear elastic model that accounts for turbulence wind effects is adequate for dynamic response of a tall, slender structure subjected to wind loads [45], the standard aerodynamic quasi-steady theory [46], based on random vibration theory and frequency domain analysis, can be used. Capitalizing on the multi-directional wind aerodynamic analysis that incorporates along-wind, across-wind and torsional load effects [47], the power spectral density (PSD) of the generalized buffeting forces $S_{Q_bQ_b}$, induced by turbulent wind with mean-wind, horizontal incidence angle Ψ, is summarized in Eqs. (1a) and (1b) below. Note that the vortex shedding loads are separately addressed in $S_{Q_vQ_v}$ by suitable correlation length L_s [47]:

$$S_{Q_bQ_b}(n) = \iint_0^h \frac{\rho^2 D^2}{4}\bar{U}(z_1)\bar{U}(z_2)\boldsymbol{\Phi}^T\boldsymbol{C}^* \times \begin{bmatrix} S_{\mathrm{uu}}(n,z_1,z_2) & 0 \\ 0 & S_{\mathrm{vv}}(n,z_1,z_2) \end{bmatrix} \boldsymbol{C}^{*,T}\boldsymbol{\Phi}\mathrm{d}z_1\mathrm{d}z_2 \tag{1a}$$

$$S_{Q_vQ_v}(n) = \frac{2L_s}{\sqrt{\pi}n_{0,y}}\int_0^h \left(\frac{1}{2}\rho\bar{U}^2(z)D\tilde{C}_L\Phi_y(z)\right)^2 \frac{n}{B_w n_s} \times \exp\left[-\left(\frac{1-n/n_s}{B_w}\right)^2\right]\mathrm{d}z \tag{1b}$$

where

$$\boldsymbol{C}^* = \begin{bmatrix} \cos\Psi & -\sin\Psi & 0 \\ \sin\Psi & \cos\Psi & 0 \\ 0 & 0 & 1 \end{bmatrix} \begin{bmatrix} 2C_D(\Psi) & C'_D(\Psi)-C_L(\Psi) \\ 2C_L(\Psi) & C'_L(\Psi)+C_D(\Psi) \\ 2DC_M(\Psi) & DC'_M(\Psi) \end{bmatrix} \tag{1c}$$

In the previous equations, $S_{Q_bQ_b}$ and $S_{Q_vQ_v}$ are the PSD matrices of the generalized buffeting forces and vortex shedding forces, respectively; $\bar{U}(z)$ is the mean wind speed at elevation z; $\boldsymbol{\Phi}$ is the mode shape matrix which may account for inter-modal coupling due to non-uniplanar, complex structural modes shapes [47]; $C_D(\Psi)$, $C_L(\Psi)$ and $C_M(\Psi)$ are the aerodynamic static coefficients of horizontal drag force, horizontal transverse lift force and torque, respectively, at mean-wind incidence angle Ψ; the derivatives with respect to Ψ are $C'_D(\Psi)$, $C'_L(\Psi)$ and $C'_M(\Psi)$, respectively; S_{uu} and S_{vv} are the cross PSD functions of the along-wind and across-wind horizontal turbulence components, respectively; ρ is the air density; D is a reference, horizontal width of the body fixture. $\tilde{C}_L$ is the standard deviation (STD) of C_L needed for vortex-shedding analysis; B_w is the bandwidth of $S_{Q_vQ_v}$; $n_s = S_t\bar{U}(z)/D$ is the vortex-shedding frequency of the wake excitation load with S_t being the Strouhal number; $n_{0,y}$ and Φ_y are the fundamental-mode natural frequency and the mode shape function in the y–z plane.

2.2. Fragility modeling and assessment

Following the general PBWE framework, composed of workflow steps that are associated with aerodynamic analysis, structural analysis, damage and loss analysis [4], fragility F_T of a structure is defined as the conditional probability that a particular engineering demand parameter, *EDP*, exceeds a pre-selected threshold T of a performance objective (i.e., limit state *LS*), if the hazard event has intensity measure *IM*:

$$F_T(IM) = P(EDP > LS|IM) \tag{2}$$

The *EDP*s for a slender monopole structure subjected to wind loads, can be chosen as the lateral deflection at the top of the tower $z = h$ since it can be directly related to the maximum overturning moment at the base and hence controls the structural design. According to the specifications for cantilevered vertical support structures in ASSHTO [48], the

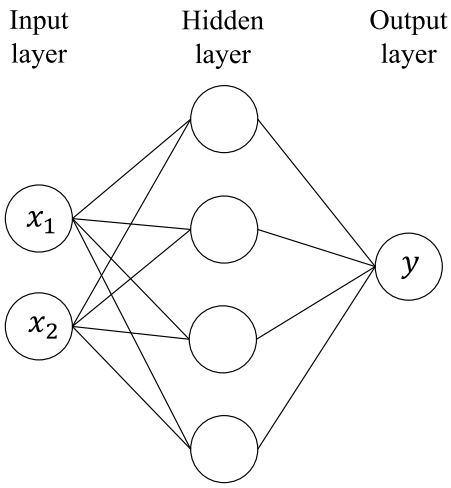

Fig. 1. Illustration of a 2-4-1 fully connected three-layer neural network.

maximum lateral deflection should be less than 10% of the total height h. Two *IM*s, used for the description of wind loads in a mixed-climate wind load, are defined: mean wind speed $\bar{U}_h$, evaluated at $z = h$ and horizontal mean-wind incidence angle Ψ.

3. Surrogate modeling with ANN

An ANN is a computer model composed of parallel processing units, i.e., neurons, interconnected by modifiable weights represented by links between units, aggregated in consecutive layers, i.e., an input layer, hidden layer(s), and an output layer [49]. Only basic descriptions will be presented, but more extensive mathematical concepts powering these computational systems are described by [50]. The input units represent the components of a feature vector, i.e., the independent variables of the problem to be solved; the output units emit a vector of final outputs, i.e., the structural response predictions. Each unit in the hidden layer computes the inner product of the inputs from the previous layer (append $x_0 = 1$) with its weights (append a bias w_{k0}), and then passes it through a nonlinear activation function that leads to the next layer. For an ANN with the architecture illustrated in Fig. 1, the generic output of the kth unit is computed as in Eq. (3) by feed-forward propagation with notation adapted from [51]:

$$\hat{y}_k = f\left(\sum_{j=1}^{n_H} w_{kj} f\left(\sum_{i=1}^{d} w_{ji} x_i + b_j\right) + b_k\right) \tag{3}$$

In Eq. (3), $\hat{y}_k$ denotes the output of the kth unit in the output layer; x_i denotes the ith unit in the input layer and w_{ji} denotes the input-to-hidden layer weights at the hidden unit j, while w_{kj} denotes the hidden-to-output layer weights at the hidden unit k; b_j and b_k denote the bias added to the input layer and the hidden layer, respectively; d and n_H denote the size of the input vector and hidden layer, respectively. $f(\cdot)$ is a transfer or activation function, a nonlinear function that nonlinearly maps inputs into a new variable space. Several options for the transfer function are available: the sigmoid function, hyperbolic tangent and the rectified linear unit (RELU) function, depending on the specific problem and training performance.

The training error, computed as the summation of the squared difference between the predicted output and the reference output, is propagated backwards using the chain rule, to determine the gradients of the error with respect to the weights and biases of the hidden units, following the iterative gradient-related optimization methods (i.e., gradient descent, stochastic gradient descent).

The task of evaluating fragilities for a structure subjected to wind loads via surrogate modeling with ANNs, is then reduced to a standard supervised learning problem. The goal is to train an ANN model, i.e., to find its optimal values for the weights and biases, such that the error between the fragilities offered by the model and those given by the reference database, is minimal. In actual training of such an ANN model, the reference dataset is divided into three parts, i.e., training set, validation set and testing set, where the training set and the validation set are explored during feedforward propagation and error backpropagation to obtain an ANN that has maximum accuracy but avoids overfitting, and the testing set is then used for performance measure on the model's generalization property.

The topology of the neural network for this study has an input layer of size equal to the number of intensity measures (i.e. $d = 2$), and an output layer consisting of just one output unit representing the structural fragility (i.e. $k = 1$). The activation function used in this study is the sigmoid function as its co-domain matches well with that of fragility. The number of neural network's hidden layers and hidden units is determined through trial and error, but is limited to small values that are associated with a shallow neural network, to avoid the problem of over-fitting that is likely to occur if unnecessarily complex models are employed for the simple case examined herein.

4. Numerical study

In this preliminary study, the fragility function of a generalized monopole point-like (plate) structure with two horizontal degrees of freedom (DOFs), subjected to turbulent wind loads induced by mixed wind climate (typical of mid-Atlantic states, with hurricanes and extra-tropical depressions), is examined. A higher-fidelity, higher-resolution dataset of structural response is first generated for fragility approximation through the BFMC method with the sampling size $N_{BFMC} = 5000$; i.e., each combination of the mean wind speed $\bar{U}_h$ at the reference elevation $z = h$ and the mean wind horizontal direction Ψ entails a total of 5000 realizations. A second, lower-fidelity, lower-resolution dataset of structural response is subsequently generated as the reference dataset for the calibration (training, validation and testing) of surrogate ANNs, whose sampling size is just 10% of the first one, i.e. $N_{MC\_ANN} = 500$. Finally, the LSAMC method with the sampling size $N_{LSAMC} = 5000$ is applied to evaluate fragilities of the structure whose results are also compared with those of ANNs.

4.1. Generalized monopole tower, point-like (plate) structure

As illustrated in Fig. 2(a), the general behavior of a slender, vertical monopole point-like (plate) structure, typical of roadway signboards and high-mast lighting structures, is described by a cantilever beam model with lumped mass m at height h, subjected to a concentrated wind load acting on the projected area A of the large fixture. It is noted that linear analysis is adequate to examine the overturning moment at base at first yielding of the tower structure and that, exceeding the yield limit of the bending stresses in the base cross section implies loss of use of the tower, and basically incipient collapse. Thus, nonlinear structural analysis is unnecessary in this study. The two-DOF, horizontal lateral motion components in the along-wind (x) and across-wind (y) directions are represented by corresponding fundamental frequencies of 0.7 Hz. Torsional effects about the z axis are neglected. The wind incidence angle Ψ, as depicted in 2(b), indicates the horizontal angle between the x-axis of the coordinate centered at the lumped mass and the direction of the concentrated drag force, ignoring other wind forces for the sake of simplicity, e.g., the static, transverse lift force and the influence of vertical turbulence component. The parameters related to vortex shedding force, as calculated by Eq. (1b), are derived through procedures recommended in ESDU 90036 [52], for a standard plate's rectangular cross section with dimensions of 4.0 m × 0.4 m. The main properties of the generalized monopole structural and load model are available in Table 1. It is noted that this simple structure is specifically selected and will suffice for the purpose of shedding light on the adaptive modeling capabilities of ANNs. A more complex structure with multiple DOFs will be examined in future studies by the authors.

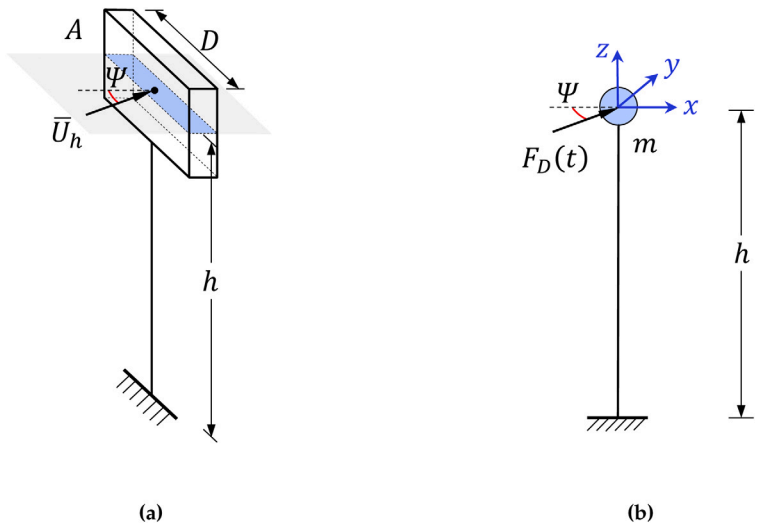

Fig. 2. Generalized monopole tower, point-like (plate) structure: (a) schematic of the structure; (b) generalized model and motion coordinates.

Table 1
Properties of the generalized 2DOF monopole (plate) structure.

Quantity	Symbol	Unit	Value
Lumped mass at $z = h$	m	[kg]	600.0
Projected area of board (or luminaire fixture)	A	[m^2]	8.0
Height	h	[m]	35.0
Reference width	D	[m]	4.0
Fundamental frequency	$n_{0,x}$, $n_{0,y}$	[Hz]	0.70
Structural damping ratio in x-plane	$\xi_{0,x}$	–	0.02
Structural damping ratio in y-plane	$\xi_{0,y}$	–	0.01
Strouhal number	S_t	–	0.125
STD of vortex shedding lift coeff. at $\Psi = 0°$	$\tilde{C}_{L0}$	–	0.245
Vortex shedding excitation correlation length	L_s	[m]	1.06
Vortex shedding excitation bandwidth parameter	B_w	–	0.06
Friction velocity when $\bar{U}_h = 50$ m/s	u_*	[m/s]	2.45
Roughness length	z_0	[m]	0.01

4.2. Description of wind load uncertainty

To account for one of the principal uncertainty sources in wind design, the drag force coefficient C_D of the wind load, as expressed in Eq. (5), is modeled as a random parameter that depends on the horizontal mean wind incidence angle Ψ, where C_{D0}, denoting the drag coefficient at zero incidence angle, is assumed as a random variable described by a normal distribution with mean $\mu_{C_{D0}} = 1.2$ and coefficient of variation $COV = 0.1$ [53]. The logarithmic profile is used to model the horizontal, mean wind speed $\bar{U}(z)$ with roughness length z_0 (Table 1). The Kaimal's model [54] is used to replicate the turbulence power spectral density function in the horizontal, along-wind and cross-wind directions, as expressed in Eqs. (4a) and (4b), respectively:

$$\frac{nS_u(z,n)}{u_*^2} = \frac{200f}{(1+50f)^{\frac{5}{3}}} \tag{4a}$$

$$\frac{nS_v(z,n)}{u_*^2} = \frac{17f}{(1+9.5f)^{\frac{5}{3}}} \tag{4b}$$

where u_* denotes the friction velocity and $f = nz/\bar{U}(z)$ denotes the Monin coordinate.

During the simulation of stochastic wind loads generated by Monte-Carlo sampling, the mean-wind incidence angle is set to 19 evenly distributed values in the range of [0°, 90°] to incorporate wind directionality effects, i.e., $\Psi \in \{0°, 5°, 10°, \ldots, 80°, 85°, 90°\}$, while the wind speed $\bar{U}_h$ is set to the range of $0 \sim 90$ m/s with an increment of 5 m/s.

$$C_D(\Psi) = C_{D0} - 0.20\,(1 - \cos 2\Psi) \tag{5}$$

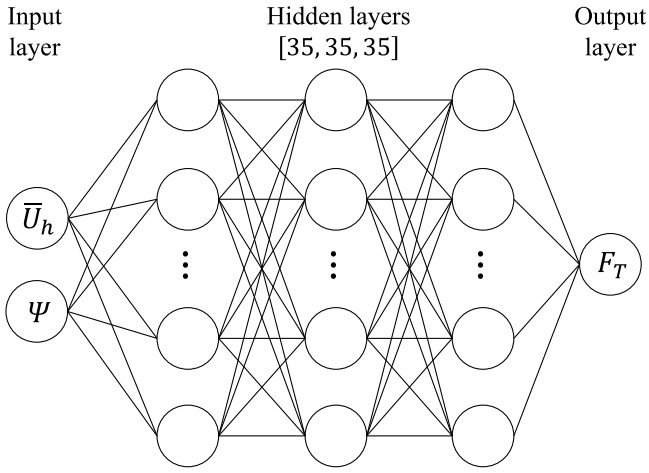

Fig. 3. "Optimized" ANN architecture with three fully connected hidden layers, found using the reference dataset.

4.3. Training of ANNs

The reference dataset for ANN calibration, comprises 1710 low-fidelity model output fragilities, i.e. 19 incidence angles × 18 mean wind velocities × 5 repetitions. The ANN training is implemented using the open source computer platform, PyTorch [55]. Specifically, the training epoch, i.e., the number of full iterations over the entire training set, is set to 200; the gradient descent algorithm utilizes a "minibatch" of size 32, a technique designed to achieve a balance between speed and accuracy of model updates [i.e., weights and biases in Eq. (3)]. The training error is quantified by the mean squared error (MSE) computed over the training set; the generalization and accuracy of the trained ANNs to unseen data is evaluated through the relative full-field error ϵ [56] given by Eq. (6)

$$\epsilon = \frac{\|\boldsymbol{y}^* - \hat{\boldsymbol{y}}\|_2}{\|\boldsymbol{y}^*\|_2} \tag{6}$$

where $\boldsymbol{y}^*$ is the reference exact value and $\|\cdot\|_2$ denotes ℓ_2 norm.

The ANN architectures, used in this study, are those with a small number of fully connected hidden layers. It has been found that a single hidden layer can capture most features of complex and nonlinear problems [57]. By adjusting the number of hidden layers and the neurons

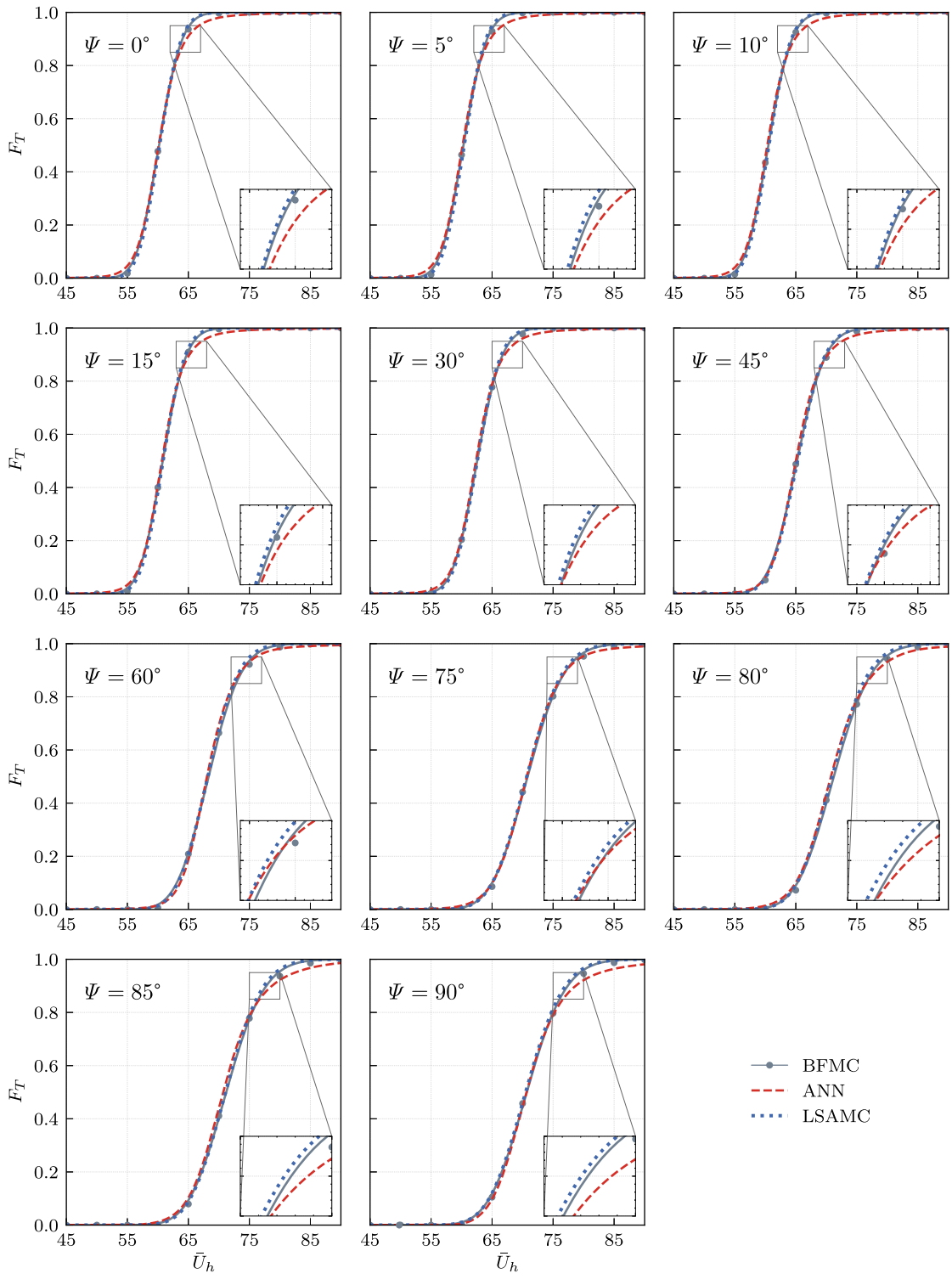

Fig. 4. Comparison of fragility F_T obtained by BFMC sampling, via ANN-based surrogate modeling and by LSAMC method.

in each layer, it is possible to find a combination that minimizes the ANN training error, based on the reference dataset generated from the low-fidelity model outputs. The procedure returned an ANN consisting of 3 hidden layers with 35 neurons each, which is illustrated in Fig. 3. As introduced earlier, the two independent, input variables are *IM*s associated with wind loads, i.e., the mean wind speed $\bar{U}_h$ at $z = h$ and the mean-wind incidence angle Ψ; the dependent output variable is the fragility or conditional exceedance probability F_T.

4.4. Examination of structural fragility results

To validate the predictions of fragility F_T found by ANN-based surrogate model, results are compared against the "exact" F_T values obtained by BFMC sampling. Comparisons are also extended to fragilities evaluated numerically by LSAMC method, which operates by layered sampling over the range of each input random variable [44], i.e., C_D in this example. Fig. 4 presents the collection of $F_T$results found by the various simulation methods. As an example, only 11 out of 19

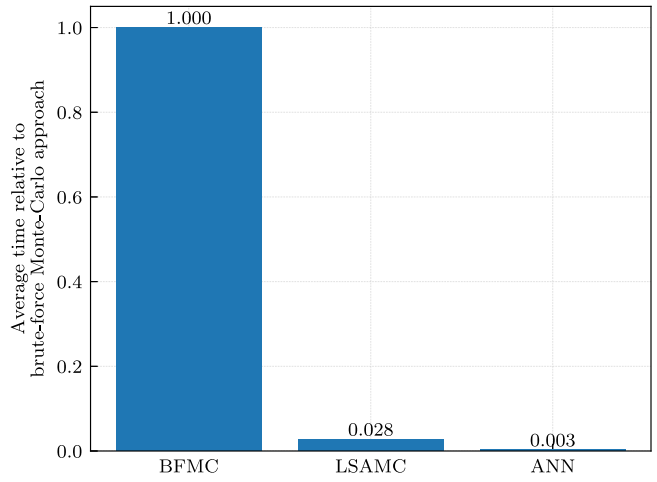

Fig. 5. Comparison of relative computing time among BFMC, LSAMC and surrogate ANN methods.

examined wind incidence angles Ψ are illustrated in the figure. The ANN-generated curves in dashed lines agree well with the reference, solid lines found by BFMC. It is also noted that LSMAC predictions in dash-dotted lines are also adequate for all the incidence angles presented. This remark confirms the promising ability of ANN-based surrogate models to capturing "unseen" features shared by the results of a higher-fidelity, higher-resolution dataset. Furthermore, even though ANNs are calibrated using a sparsely-sampled reference dataset, ANN models can still reasonably and accurately evaluate F_T depending on the *IM*s. Finally, the encouraging propensity to model generalization of a properly calibrated ANN can be superior in evaluating high-fidelity interpolations of fragility with multi-dimensional input variables.

A closer examination near the tail of the fragility curves in Fig. 4 reveals certain discrepancies between the ANN results and the reference results. This behavior may be primarily due to the lack of data points specifically near the transition range of fragility curves where slope drops quickly, resulting in a temporary "shutdown" of ANNs to fully capture the sharp transition in fragilities before leveling out at 1.0. Improvements can be made by using more complex network architectures with a larger number of hidden layers and more neurons in each layer, but this would risk over-fitting. Another measure is to increase the local resolution around the transition area of fragilities without increasing the resolution of the reference database, thus avoiding the accompanying significant rise in computing cost. As the priority of this study focuses on the application of ANNs within the PBWE framework, differences of the ANN results will be further investigated in future studies.

Fig. 5 presents the average computing time, performed on a 32-core standard workstation, relative to the BFMC method. It is revealing that the LSAMC method has achieved an extraordinary computational gain by reducing the computing time to just 2.8% of the BFMC method. More interestingly, the ANN powered surrogate models performed even better by cutting the computing time to less than 1% of the brute-force approach. The primary contribution to the savings of ANN model comes from the fact that the computing cost needed to derive a low-resolution database is much smaller, compared to that of a high-resolution database.

5. Conclusions

This communication examined the systematic applicability of ANNs as surrogate models to alleviate the computational burden of the standard PBWE simulation framework. A slender monopole tower structure subjected to mixed-climate wind load was examined. Two datasets of wind-induced structural response were separately generated: a high-fidelity, high-resolution dataset used by both BFMC and LSAMC methods, and a low-fidelity, low-resolution dataset derived for the calibration of ANN-based surrogate models. A shallow ANN with two inputs, the mean wind velocity and direction at the tower top, and internal layers composed of 3 fully connected layers with 35 neurons each, was determined through optimization. The ANN-powered surrogate results exhibit adequate accuracy compared with the high-fidelity results while cutting the computing time to less than 1% of the high-fidelity results; this suggests the great promise to incorporate the surrogate ANN modeling in a PBWE framework. Future investigation is anticipated to expand application of surrogate ANN models to more complex structures.

Declaration of competing interest

The authors declare that they have no known competing financial interests or personal relationships that could have appeared to influence the work reported in this paper.

Data availability

Data will be made available on request.

Acknowledgments

The Authors would like to acknowledge the collaboration of Professors Bernardo Barbiellini from Lappeenranta University of Technology, Finland and Gian Felice Giaccu from the University of Sassari, Italy for the LSAMC formulation. This material is based upon work supported in part by the National Science Foundation (NSF) of the United States of America under grant CMMI-1852678 in 2019–2023. Any opinions, findings and conclusions or recommendations are those of the authors and do not necessarily reflect the views of the NSF.

References

[1] Griffis LG. Serviceability limit states under wind load. Eng J 1993;30(1):1–16.
[2] Unanwa C, McDonald J, Mehta K, Smith D. The development of wind damage bands for buildings. J Wind Eng Ind Aerodyn 2000;84(1):119–49.
[3] Ellingwood B, Rosowsky D, Li Y, Kim J. Fragility assessment of light-frame wood construction subjected to wind and earthquake hazards. J Struct Eng ASCE 2004;130(12):1921–30.
[4] Ciampoli M, Petrini F, Augusti G. Performance-based wind engineering: towards a general procedure. Struct Saf 2011;33(6):367–78.
[5] Ciampoli M, Petrini F. Performance-based aeolian risk assessment and reduction for tall buildings. Probab Eng Mech 2012;28:75–84.
[6] Bernardini E, Spence SM, Kareem A. A probabilistic approach for the full response estimation of tall buildings with 3D modes using the HFFB. Struct Saf 2013;44:91–101.
[7] Spence SM, Gioffrè M. Large scale reliability-based design optimization of wind excited tall buildings. Probab Eng Mech 2012;28:206–15.
[8] Cui W, Caracoglia L. Simulation and analysis of intervention costs due to wind-induced damage on tall buildings. Eng Struct 2015;87:183–97.
[9] Cui W, Caracoglia L. Performance-based wind engineering of tall buildings examining life-cycle downtime and multisource wind damage. J Struct Eng ASCE 2020;146(1):04019179.
[10] SEAOC. Vision 2000: Performance based seismic engineering of buildings. Tech. rep., Sacramento, California, USA: Structural Engineers Association of California; 1995.
[11] Jaynes ET. Probability theory: the logic of science. Cambridge University Press; 2003.
[12] van de Lindt JW, Dao TN. Performance-based wind engineering for wood-frame buildings. J Struct Eng ASCE 2009;135(2):169–77.
[13] Jain A, Srinivasan M, Hart GC. Performance based design extreme wind loads on a tall building. Struct Des Tall Build 2001;10(1):9–26.
[14] Seo D-W, Caracoglia L. Estimating life-cycle monetary losses due to wind hazards: Fragility analysis of long-span bridges. Eng Struct 2013;56:1593–606.
[15] Augusti G, Ciampoli M. Performance-based design in risk assessment and reduction. Probab Eng Mech 2008;23(4):496–508.
[16] Au SK, Beck J. Subset simulation and its application to seismic risk based on dynamic analysis. J Eng Mech 2003;129(8):901–17.

[17] Tsompanakis Y, Lagaros ND, Papadrakakis M. In: Frangopol DM, editor. Structural design optimization considering uncertainties: structures & infrastructures book. Series, vol. 1, CRC Press; 2008.
[18] Gavin HP, Yau SC. High-order limit state functions in the response surface method for structural reliability analysis. Struct Saf 2008;30(2):162–79.
[19] Jia G, Taflanidis AA. Kriging metamodeling for approximation of high-dimensional wave and surge responses in real-time storm/hurricane risk assessment. Comput Methods Appl Mech Engrg 2013;261:24–38.
[20] Kroetz HM, Tessari RK, Beck AT. Performance of global metamodeling techniques in solution of structural reliability problems. Adv Eng Softw 2017;114:394–404.
[21] Taflanidis AA, Jia G, Gidaris I. Natural hazard probabilistic risk assessment through surrogate modeling. In: Multi-hazard approaches to civil infrastructure engineering. Springer; 2016, p. 59–86.
[22] De Grandis S, Domaneschi M, Perotti F. A numerical procedure for computing the fragility of NPP components under random seismic excitation. Nucl Eng Des 2009;239(11):2491–9.
[23] Seo J, Dueñas-Osorio L, Craig JI, Goodno BJ. Metamodel-based regional vulnerability estimate of irregular steel moment-frame structures subjected to earthquake events. Eng Struct 2012;45:585–97.
[24] Saha SK, Matsagar V, Chakraborty S. Uncertainty quantification and seismic fragility of base-isolated liquid storage tanks using response surface models. Probab Eng Mech 2016;43:20–35.
[25] Krishnamurthy T. Response surface approximation with augmented and compactly supported radial basis functions. In: 44th AIAA/ASME/ASCE/AHS/ASC structures, structural dynamics, and materials conference. 2003, p. 1748.
[26] Gidaris I, Taflanidis AA, Mavroeidis GP. Kriging metamodeling in seismic risk assessment based on stochastic ground motion models. Earthq Eng Struct Dyn 2015;44(14):2377–99.
[27] Moustapha M, Bourinet J-M, Guillaume B, Sudret B. Comparative study of kriging and support vector regression for structural engineering applications. ASCE-ASME J Risk Uncertain Eng Syst A 2018;4(2).
[28] Gharehbaghi S, Yazdani H, Khatibinia M. Estimating inelastic seismic response of reinforced concrete frame structures using a wavelet support vector machine and an artificial neural network. Neural Comput Appl 2020;32(8):2975–88.
[29] Segura R, Padgett JE, Paultre P. Metamodel-based seismic fragility analysis of concrete gravity dams. J Struct Eng 2020;146(7).
[30] De Lautour OR, Omenzetter P. Prediction of seismic-induced structural damage using artificial neural networks. Eng Struct 2009;31(2):600–6.
[31] Wu T, Kareem A. Modeling hysteretic nonlinear behavior of bridge aerodynamics via cellular automata nested neural network. J Wind Eng Ind Aerodyn 2011;99(4):378–88.
[32] Mitropoulou CC, Papadrakakis M. Developing fragility curves based on neural network IDA predictions. Eng Struct 2011;33(12):3409–21.
[33] Abdellatif M, Atherton W, Alkhaddar R, Osman Y. Flood risk assessment for urban water system in a changing climate using artificial neural network. Nat Hazards 2015;79(2):1059–77.
[34] Kim T, Song J, Kwon O-S. Probabilistic evaluation of seismic responses using deep learning method. Struct Saf 2020;84:101913.
[35] Le V, Caracoglia L. A neural network surrogate model for the performance assessment of a vertical structure subjected to non-stationary, tornadic wind loads. Comput Struct 2020;231:106208.
[36] Micheli L, Hong J, Laflamme S, Alipour A. Surrogate models for high performance control systems in wind-excited tall buildings. Appl Soft Comput 2020;90:106133.
[37] Chuang W-C, Spence SM. Rapid uncertainty quantification for non-linear and stochastic wind excited structures: a metamodeling approach. Meccanica 2019;54(9):1327–38.
[38] Wang H, Wu T. Knowledge-enhanced deep learning for wind-induced nonlinear structural dynamic analysis. J Struct Eng 2020;146(11):04020235.
[39] Tsai L-W, Alipour A. Physics-informed long short-term memory networks for response prediction of a wind-excited flexible structure. Eng Struct 2023;275:114968.
[40] Li T, Wu T, Liu Z. Nonlinear unsteady bridge aerodynamics: Reduced-order modeling based on deep LSTM networks. J Wind Eng Ind Aerodyn 2020;198:104116.
[41] Li B, Spence SM. Metamodeling through deep learning of high-dimensional dynamic nonlinear systems driven by general stochastic excitation. J Struct Eng 2022;148(11):04022186.
[42] Xue J, Xiang Z, Ou G. Predicting single freestanding transmission tower time history response during complex wind input through a convolutional neural network based surrogate model. Eng Struct 2021;233:111859.
[43] Adeli H. Neural networks in civil engineering: 1989–2000. Comput-Aided Civ Infrastruct Eng 2001;16(2):126–42.
[44] Zhang L, Caracoglia L. Layered stochastic approximation Monte-Carlo method for tall building and tower fragility in mixed wind load climates. Eng Struct 2021;239:112159.
[45] Davenport AG. The response of supertall buildings to wind. In: Second century of the skyscraper. Springer; 1998, p. 705–25.
[46] Davenport AG. The application of statistical concepts to the wind loading of structures.. Proc Inst Civ Eng 1961;19(4):449–72.
[47] Cui W, Caracoglia L. A fully-coupled generalized model for multi-directional wind loads on tall buildings: A development of the quasi-steady theory. J Fluids Struct 2018;78:52–68.
[48] AASHTO. 2017 interim revisions to the LRFD specifications for structural supports for highway signs, luminaires, and traffic signals. Tech. rep. LRFDLTS-1, Washington, DC, USA: American Association of State Highway Transportation Officials; 2016.
[49] Hornik K, Stinchcombe M, White H. Multilayer feedforward networks are universal approximators. Neural Netw 1989;2(5):359–66.
[50] Rumelhart DE, McClelland JL. Learning internal representations by error propagation. In: Parallel distribution processing: explorations in the microstructure of cognition: foundations. MIT Press; 1987, p. 318–62, URL http://ieeexplore.ieee.org/document/6302929.
[51] Dongmei H, Shiqing H, Xuhui H, Xue Z. Prediction of wind loads on high-rise building using a BP neural network combined with POD. J Wind Eng Ind Aerodyn 2017;170:1–17.
[52] ESDU. Structures of non-circular cross section: dynamic response due to vortex shedding. Engineering Sciences Data Unit, Data Item 90036; 1990.
[53] Le V, Caracoglia L. Computationally efficient stochastic approach for the fragility analysis of vertical structures subjected to thunderstorm downburst winds. Eng Struct 2018;165:152–69.
[54] Kaimal JC, Wyngaard J, Izumi Y, Coté O. Spectral characteristics of surface-layer turbulence. Q J R Meteorol Soc 1972;98(417):563–89.
[55] PyTorch: An open source machine learning framework that accelerates the path from research prototyping to production deployment. 2021, https://pytorch.org/, accessed: 2021-04-30.
[56] Ren P, Rao C, Liu Y, Wang J, Sun H. PhyCRNet: Physics-informed convolutional-recurrent network for solving spatiotemporal PDEs. 2021, arXiv preprint arXiv:2106.14103.
[57] Khanduri A, Bédard C, Stathopoulos T. Modelling wind-induced interference effects using backpropagation neural networks. J Wind Eng Ind Aerodyn 1997;72:71–9.